Macromolecules
ARTICLE

Retarded Crystallization in Polyamide/Layered Silicates Nanocomposites caused by an Immobilized Interphase

Andreas Wurm,*,[†] Mohamed Ismail,[†] Bernd Kretzschmar,[‡] Doris Pospiech,[‡] and Christoph Schick[†]

[†]*University of Rostock, Institute of Physics, Wismarsche Strasse 43-45, 18051 Rostock, Germany and* [‡] *Leibniz Institute of Polymer Research Dresden, P.O. Box 120 411, 01005 Dresden, Germany*

ABSTRACT: The interphase between the inorganic filler and the polymer matrix is considered as one of the most important parameters for inorganic/polymer nanocomposites. In nanocomposites based on semicrystalline polymers we have to take into account two, often immobilized, interphases. One is existing between the polymer crystals and the amorphous part of the polymer and another one between the inorganic filler and the polymer matrix. The fraction of immobilized interphases, the rigid amorphous fraction (RAF), is available from specific heat capacity at the glass transition region of the nanocomposites. Assuming a certain constant amount of RAF around the individual lamellar crystals, which is available from the pure semicrystalline polymer, we determined the RAF related to the inorganic nanofiller. For the polyamide 6/layered silicate nanocomposites studied the RAF due to the filler reached more than 25% of the polymer fraction. The existence of a RAF around the nanofiller finally explains the observed reduced crystallinity in the polymer and the retarded nonisothermal crystallization of the polyamide 6 in the nanocomposites.

1. Introduction

Filling polymers with inorganic particles is used to improve the stiffness of the materials, to reinforce thermal and mechanical properties as well as the chemical stability, to enhance the resistance to fire, decrease the gas permeability etc., see[1] for a review. On the other hand, addition of only a small amount of inorganic particles influences crystallization kinetics during processing of semicrystalline polymers. The particles often act as nucleating agents[2,3] but also retardation of crystallization has been observed.[4,5] Sometimes, decrease or increase of the overall growth rate depends on filler concentration.[6–9]

Despite the wide application of polymer/inorganic nanocomposites the basic understanding of the interaction between the polymer and the inorganic filler is still lacking. Modification of the structure and dynamics of the polymer at and near the particle surface is considered important.[10,11] Because of the large surface area this interphase should contribute significantly to the properties of the nanocomposite, even at low filler content. Most probably chain connectivity and mobility in the interphase defines the overall properties of the composite. Particularly important for the nanocomposite properties is a good adhesion between nanoparticles and the polymer matrix. It is assumed that the existence of an immobilized amorphous polymer fraction around the nanoparticles could actually enhance this adhesion, thus resulting in improved impact strength (toughness).

Obtaining information about mobility of different fractions in the polymer needs experimental methods which are sensitive to the dynamics of the polymer chains and which can be easily applied to multicomponent systems. Differential scanning calorimetry (DSC) is such a technique, and it is widely used to characterize polymer nanocomposites. Changes in crystallization, melting and glass transition behavior can be detected and

have been reported frequently. However, so far only minor attention has been paid to deduce the existence of an interphase in inorganic/polymer nanocomposites from DSC curves. Privalko et al.[12,13] used specific heat capacity to identify a fraction of reduced mobility in nanocomposites. Pissis et al.[14,15] applied different relaxation experiments like dielectric spectroscopy and TSDC (thermally stimulated depolarization current) to determine an immobilized fraction in different nanocomposites. In this paper we extend our previous studies[16] on heat capacity measurements for nanocomposites of amorphous polymer matrices to nanocomposites consisting of a semicrystalline polymer matrix, particularly polyamide 6 (PA6). To identify an immobilized interphase of the polymer a formalism was applied which is well established for the determination of a rigid amorphous fraction (RAF) in semicrystalline polymers, and described in detail by Wunderlich et al.[17,18] The existence of a rigid amorphous fraction in poly(methyl methacrylate) (PMMA)/SiO_2 nanocomposites based on heat capacity measurements at the glass transition of the polymer has already been shown. The immobilized polymer layer around the particles was estimated to be about 2 nm thick. For the system polystyrene (PS)/SiO_2, an immobilized layer could not be detected, implying that the existence, size, and properties of the organic/inorganic interphase varies between different composites.

No universal picture can be drawn; each nanocomposite has to be treated individually with respect to its components (polymer, filler, chemical modification, or other additives) and preparation (filler modification, dispersion, processing). The study reported in ref 16 focused on amorphous polymers and its nanocomposites. In this paper, we report heat capacity measurements of nanocomposites with crystallizable polymers, in particular polyamides (PA). We will discus rigid amorphous fractions of two different origins. One rigid amorphous fraction is originated from the filler, as described above for an amorphous matrix. The second fraction of rigid amorphous polymer material is caused by

*Corresponding author. Telephone: +49-381-498 6884. Fax: +49-381-498 6882. E-mail: andreas.wurm@uni-rostock.de.

the restriction of mobility of the amorphous material due to the polymer crystals. The methodology for determination of these fractions of different mobility from heat capacity and its limitations are described.

Finally, based on the occurrence of two interphases we will provide an explanation of the observed reduction of crystallinity of the polymer fraction and retardation of nonisothermal crystallization for PA6/layered silicate nanocomposites.

2. Experimental Section

2.1. Materials. The polymer matrix Polyamide 6 (Aquamid AQ500) was supplied by Aquafil Technopolymers. Before the compounding tests it was dried to a water content lower than 0.1 wt %. In this dry state the melt volume rate of PA6 was 62 cm^3/10 min at the processing temperature of 240 °C and a load of 5 kg (according DIN EN ISO 1133). The organophilically modified MMT Nanofil 9 is stearylbenzyldimethylammonium chloride modified montmorillonite purchased from Rockwood Additives as a powder with a medium particle size of 8 μm. Inorganic clay content is 66 wt % of the total filler content and the layer distance between the platelets is 2.1 nm. Pursuant to the data sheet of the manufacturer the MMT has a primary particle size after complete exfoliation of 100−500 nm in lateral directions and a thickness of about 1 nm. The powder was also predried before compounding.

Nanocomposites have been melt-mixed at 240 °C for 5 min using a 15 cm^3 microcompounder (DSM, Geleen, Nl) with a screw speed of 100 min^{-1}. Beside the pure polymer, nanocomposites with Nanofil 9 content between 3.3 and 60.8 wt % have been produced. Resulting inorganic content, which is given in the sample names, was between 2.2 and 40 wt %. The difference between filler and inorganic content is due to the organic modifier in the Nanofil 9.

2.2. Calorimetry. Heat capacity curves were obtained using a PerkinElmer PYRIS Diamond DSC. Samples were heated to the melt for ensuring uniform conditions at the beginning, followed by cooling at 10 K/min to the crystallization temperature or for nonisothermal crystallization to −50 °C. Precise heat capacity at T_g was determined from the following StepScan differential scanning calorimetry (SSDSC) run, a special variant of temperature modulated DSC. Measurements were performed using samples of about 20 mg, 2 K steps at heating rate 6 K/min and isotherms of about 1.5 min.[16,19] The temperature range, if not other indicated, was from −50 (below T_g) to +250 °C (above T_m). The instrument was calibrated as recommended by GEF-TA[20] by indium and zinc at zero heating rate for temperature and by sapphire for heat capacity.

For the enthalpy relaxation experiments at annealing below T_g a Perkin-Elmer DSC6, applying the identical calibration procedure was used in the common way.[21] Samples were isothermally crystallized at 200 °C until crystallization resulted in a metastable semicrystalline structure, followed by cooling with 10 K/min to the annealing temperature of 30 °C. After annealing time of 4 h, the sample was cooled at 10 K/min to −20 °C, followed by two heating runs at 10 K/min between −20 and +150 °C. Cooling rate in between was 10 K/min too. Specific enthalpy change caused by annealing can be calculated by integrating the heat capacity difference between the two heating runs in the glass transition region.

3. Results

3.1. Determination of the Rigid Amorphous Fraction at Glass Transition. The mobile amorphous fraction is defined as the polymer, which behaves liquid like, e.g., vitrifies or devitrifies in the common glass transition region (T_g) and contributes therefore to the heat capacity step at T_g. The solid fraction (SF) does not vitrify or devitrify at the common glass transition and is composed of crystalline and glassy

material. A more detailed view on the states of condensed matter in polymers has been given by Wunderlich.[22,23]

Ideally, the different fractions of mobility in semicrystalline polymers can be determined from one single DSC temperature scan. The mobile amorphous fraction (MAF) can be calculated from the heat capacity increment at T_g according to eq 1:

$$\text{MAF} = \Delta c_p / \Delta c_{p(\text{am})} \qquad (1)$$

where Δc_p is the measured heat capacity increment at T_g of the semicrystalline sample and $\Delta c_{p(\text{am})}$ is the heat capacity increment of a totally amorphous sample. The crystalline fraction (CF) can be calculated from melting enthalpy according eq 2

$$\text{CF} = \Delta h / \Delta h_0 \qquad (2)$$

where Δh is the enthalpy of fusion from integration of the heat capacity in the melting region and Δh_0 is the enthalpy of fusion for a 100% crystalline material at the same temperature. Whereas $\Delta c_{p(\text{am})}$ is sometimes experimentally accessible for quenched polymers, Δh_0 must always be taken from extrapolations and is for more than 200 polymers available from ATHAS database.[24] For polyamides which crystallize relatively fast and completely amorphous samples cannot be produced under the experimental conditions of a DSC measurement, $\Delta c_{p(\text{am})}$ can be taken from ATHAS database too. Because of the relatively broad glass transition region and the small heat capacity step for semicrystalline polymers, the accuracy of Δc_p from a standard temperature scan DSC experiment is low. TMDSC, or StepScan DSC, allows more precise determination of Δc_p but Δh cannot be achieved.[25] Therefore, Δh in this study was either calculated from cooling curves at 10 K/min for nonisothermal crystallization or from a normal DSC heating scan at 10 K/min after isothermal crystallization, while Δc_p was obtained from a separate TMDSC−StepScan measurement. Before each experiment the sample was heated to the melt at 250 °C, held there for 5 min to erase thermal history, followed by cooling to 200 °C, and annealed there for 8 h for isothermal crystallization toward a metastable structure. After annealing, the sample was further cooled to −50 °C followed by the temperature scan of interest. Identical thermal treatment including erasure of thermal history in the melt before normal scan and StepScan measurements leads to the assumption of an identical structure at the beginning of the scans. Values for Δc_p and Δh, or MAF and CF, respectively, can be taken to calculate RAF according eq 3 under the assumption of a "3-phase-model" for semicrystalline polymers:

$$\text{RAF} = 1 - \text{MAF} - \text{CF} \qquad (3)$$

The heat capacity from a StepScan experiment of pure semicrystalline PA6 in the glass transition region is shown in Figure 1 as curve a.

For semicrystalline polymers, it is well-known that the observed step in heat capacity, Δc_p, at the glass transition is often less than expected from crystallinity. Wunderlich et al.[26] therefore introduced the concept of a rigid amorphous fraction (RAF) according eq 3. From a temperature scan to the melt or during crystallization on cooling, the heat of fusion can be obtained by integrating the endothermic or exothermic peak. For the PA6 sample shown in Figure 1 one obtains a crystalline fraction of 0.3 from the enthalpy of crystallization, see Figure 2. The expected heat capacity step at T_g is than 0.7 of the step found in the completely
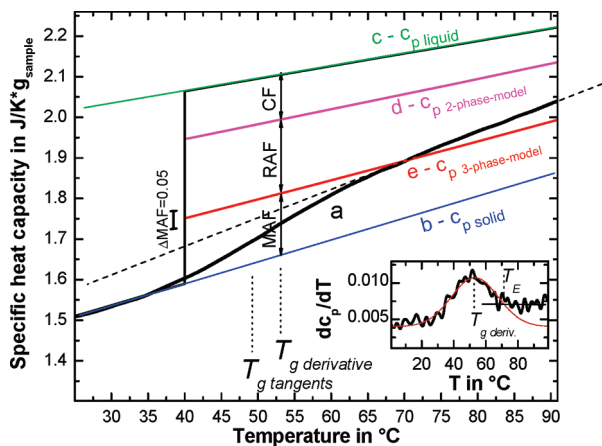
Figure 1. Specific heat capacity of PA6 in the glass transition region: (a) measured curve for a semicrystalline sample,; (b) solid ($c_{p\text{ solid}}$) and (c) liquid ($c_{p\text{ liquid}}$) reference curves from ATHAS database;[24] (d) expected specific heat capacity from a 2-phase model using the crystalline fraction from the heat of crystallization of 0.3; (e) calculated from a 3-phase model assuming an amount of 0.66 solid material. The dashed line is the tangent on the measured curve used for conventional evaluation of the glass transition, see text for discussion. The inset shows the temperature derivative of the measured specific heat capacity in $J/(g\,K^2)$ and the Gauss fit to the curve.
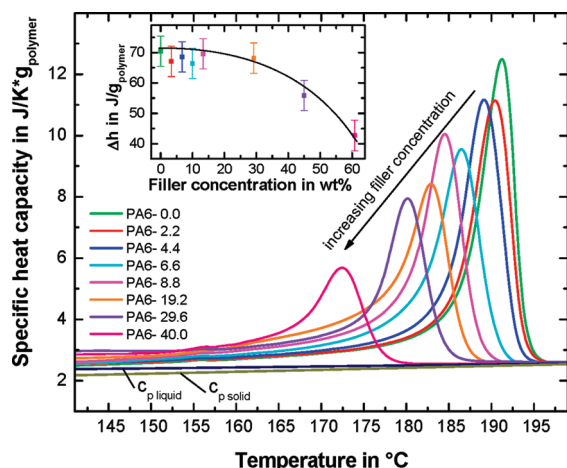

Figure 2. Specific heat capacity of PA6 and its nanocomposites during nonisothermal crystallization on cooling with 10 K/min from the melt at 250 °C from DSC scan experiments, normalized to the polymer mass fraction. The inset shows crystallization enthalpies, normalized to the polymer mass fraction, as a function of filler concentration.

amorphous PA6, assuming a 2-phase-model. Curve (**b**) presents the expected specific heat capacity assuming a 2-phase-model and is calculated as a simple superposition of the heat capacities for amorphous ($c_{p(\text{amorph})}$) and crystalline ($c_{p(\text{crystal})}$) fraction (AF and CF) according eq 4.

$$c_{p(\text{2-phase-model})} = c_{p(\text{amorph})} \times (1 - \text{CF}) + c_{p(\text{crystal})} \times \text{CF} \quad (4)$$

Obviously the experimentally determined step is significantly smaller than expected from the 2-phase-model. Therefore, a 3-phase-model, including RAF, has to be applied. The above-described algorithm for calculation of the RAF is only applicable if the baseline heat capacity is measured and no additional processes, except glass transition of the MAF, are present in the temperature range around T_g. Additional processes might be nonreversing or reversing melting or successive devitrification of the RAF. A simple superposition for liquid and solid heat capacities,

similar to eq 4, should fit the measured curve above T_g using SF instead of CF. Such a curve is shown in Figure 1 as curve e. Comparing the steeper slope of the measured heat capacity in comparison with the slopes of liquid and solid heat capacities implies that this method is not easily applicable in the present case. A non-negligible contribution to the measured heat capacity must be either an excess heat capacity in addition to the baseline heat capacity or due to a continued extension of the glass transition toward higher temperatures (successive devitrification of the RAF). An excess heat capacity could originate from a reversing melting-crystallization processes as described in.[27−31] This large slope results in another problem, namely the evaluation of the glass transition itself. Standard methods for glass transition evaluation use tangents at the heat capacity curve above and below the glass transition region. The glass transition temperature T_g can be defined as the temperature at which the measured heat capacity curve equals the half distance between the tangents. Then, the relaxation strength Δc_p is defined as the difference between the tangents at T_g. [We are using the term "relaxation strength" for describing the height of the heat capacity step at glass transition. The experimental method applied is Temperature Modulated DSC (TMDSC), which tests the relaxation behavior of the supercooled liquid and not the thermodynamic transition of the glass into the liquid. This is in accordance with relaxation experiments like DMA or dielectric spectroscopy.] In Figure 1 the tangent below glass transition coincides with the heat capacity of the solid. The tangent, best fitting the measured curve above the glass transition range, is given as the dashed line. Using this construction T_g and Δc_p are determined as $T_{g(\text{tangents})} = 48$ °C and $\Delta c_{p(\text{tangents})} = 0.12$ J/(g K). Because of the appearance of an excess heat capacity or the continuous devitrification of the RAF just above T_g this method obviously fails, because the tangent above T_g is mainly determined by the processes responsible for the large slope of the heat capacity curve. This tangent can therefore not be used for evaluation of the glass transition and, consequently, calculating MAF at T_g. We had therefore to find a more objective way of defining T_g and Δc_p from the measured heat capacity curve above the glass transition.

Assuming a 3-phase-model a superposition of the heat capacities of the three fractions represents baseline heat capacity according eq 5.

$$c_{p(\text{b})} = \text{MAF} \times c_{p(\text{am})} + \text{CF} \times c_{p(\text{cr})} + \text{RAF} \times c_{p(\text{ra})} \quad (5)$$

Above the glass transition, the heat capacity of the MAF equals liquid c_p and heat capacity of the CF solid c_p. Because RAF is assumed to be in the glassy state above glass transition of the MAF, its heat capacity equals solid c_p too. Equation 5 can be simplified to

$$c_{p(\text{b})} = \text{MAF} \times c_{p(\text{liquid})} + (\text{CF} + RAF) \times c_{p(\text{solid})} \quad (6)$$

or further to

$$c_{p(\text{b})} = \text{MAF} \times c_{p(\text{liquid})} + (1 - \text{MAF}) \times c_{p(\text{solid})} \quad (7)$$

Equations 6 and 7 represent a superposition of heat capacities of the liquid and solid fractions of the polymer. Choosing values between 0 and 1 for MAF and taking database values for $c_{p(\text{liquid})}$ and $c_{p(\text{solid})}$, certain straight lines can be constructed between liquid and solid heat capacities. But which heat capacity superposition or which value for MAF, respectively, represents the true heat capacity at the

end of the glass transition? To find out this, the end temperature of glass transition has to be defined first, which is not without problems because of possible excess contributions to the measured heat capacity.

Therefore, we decided to use the derivative of the measured heat capacity (inset in Figure 1) to determine the end temperature T_E of the glass transition. The heat capacity at the glass transition is often well described by a Gaussian error integral.[32] Then the temperature derivative of c_p corresponds to a Gauss distribution function. Deviations from the Gauss peak can be used to determine the end of the glass transition interval. Applying this to Figure 1 yields $T_E = 72\ ^\circ$C. The heat capacity value at this temperature can be assumed equal to the heat capacity of the sample with the entire MAF being in its liquid state. All other contributions, like reversing melting or a continuous devitrification of the RAF above T_g, leading to the large slope of the measured heat capacity above T_g are this way excluded from the calculation. Assuming the measured specific heat capacity at $T_E = 72\ ^\circ$C is equal to the value of the sample with the entire MAF being in its liquid state finally results in line e as the relevant curve for determination of the parameters at the glass transition. The expected heat capacity for a 3-phase-model (curve e), assuming liquid heat capacity for the MAF and solid heat capacity for CF as well as RAF, is calculated in analogy to eq 4 by replacing CF by SF. The MAF is, as indicated in the graph, represented by the difference between the heat capacity lines for the solid and the 3-phase-model, the CF by the difference between liquid heat capacity and the 2-phase-model and the RAF by the difference between 2- and 3-phase-model. Now the determined glass transition temperature is $T_{g(\text{derivative})} = 53\ ^\circ$C and the step height $\Delta c_{p(\text{derivative})} = 0.15\ \text{J/(g K)}$, significantly larger as determined using the commonly chosen tangent above T_g. Calculated MAF according eq 1 and taking $\Delta c_{p(\text{am})}$ for the amorphous sample from the ATHAS values of 0.462 J/(g K) at 48 °C and 0.452 J/(g K) at 53 °C is than 0.26 for the tangents method and 0.33 for the derivative method. Calculating RAF from MAF and CF (0.3) one receives 0.44 and 0.37. The error of MAF and RAF is relatively high because of the described evaluation difficulties and assumptions regarding heat capacity at the end of the glass transition of the MAF. For the example of pure PA6 an absolute error of about ±0.05 for MAF and RAF has to be considered. The error in the estimation of the baseline heat capacity line for the 3-phase-model can be therefore assumed to be less than 0.05 J/(g K) at T_g. Because the same algorithm for data treatment is employed and the behavior of the different samples regarding excess heat capacity is similar the relative error for different filled samples becomes smaller.

As shown in refs 16 and 33, basically the same formalism can be applied for polymer nanocomposites, taking into account the filler as an additional solid fraction. In ref 16, a RAF due to the interaction between the polymer and the inorganic filler particles was observed. Assuming a similar situation for the filled semicrystalline polymer two origins for the RAF must be considered. In this case, RAF is then always the total RAF, consisting of RAF originated by the immobilization of the amorphous phase at crystals and RAF caused by immobilization of the amorphous phase at the nanofiller surface.

Because of the difficulties regarding determination of Δc_p a method is needed which is independent of the choice of any tangents, but provides similar information about the MAF. Annealing experiments in the glass transition region provide such an independent way of determination of molecular mobility, see ref 34 for a review. The annealing causes enthalpy relaxation toward the equilibrium at and below T_g. For the evaluation no tangent construction is needed and consequently some of the difficulties described above can be avoided.[21] With annealing experiments, one makes use of the time dependence of properties of supercooled polymers during annealing at constant temperature. Amorphous materials, which are in a nonequilibrium state, relax toward equilibrium. The corresponding reduction in specific enthalpy for pure amorphous polymers and nanofilled systems should depend on the mobile amorphous material only. For the annealing experiments first a metastable semicrystalline structure was created as described above. Next, the sample was cooled with 10 K/min to the chosen annealing temperature near T_g and annealed there for a specific time. The annealing temperature for the results presented in this work was 30 °C and the annealing time was 4 h. After cooling at 10 K/min to −20 °C, the heating run to identify the enthalpy change due to the annealing was carried out at 10 K/min to 150 °C. For calculating the specific enthalpy change during annealing a baseline is needed. Therefore, the sample was cooled again with 10 K/min to −20 °C, followed by a second identical heating scan to 150 °C without annealing. The typical annealing effect can be seen in Figure 5 in the inset, lower part, as the additional endothermic contribution at glass transition, which is not present in the second heating without annealing. From both curves the excess heat capacity can be obtained by using the second heating as baseline for the heat capacity determination in the Pyris software, see inset in Figure 5, upper part.

3.2. Rigid Amorphous Fraction in PA/MMT Nanocomposites. First, the influence of organophilically modified MMT on nucleation and crystallization kinetics of PA6 was checked. Isothermal crystallization experiments for PA6 and its nanocomposites at different annealing temperatures between melting and glass transition temperature can provide this information. The high temperature range is accessible by DSC, the lower temperatures only by fast scanning calorimetry, as described in ref 35. From such large set of data a crystallization kinetics map could be derived. A much shorter way to get first information about kinetics of nucleation and crystallization from DSC experiments is nonisothermal crystallization on cooling from the melt. Differences in nucleation kinetics can be seen from differences in the crystallization onset temperature. Specific heat capacities, normalized to the polymer mass fraction, during nonisothermal crystallization on cooling of PA6 and its nanocomposites at 10 K/min are presented in Figure 2.

The onset of crystallization on cooling for the pure PA6 is 196 °C. It decreases successively with increasing filler concentration to 180 °C for the highest organophilically modified MMT content. This remarkable difference leads to the conclusion, that the presence of modified MMT reduces crystallization rate. Furthermore, the crystallization enthalpy, which can be calculated by integrating the crystallization peaks, shows a decreasing heat release during crystallization with increasing filler content too. The calculated values for the crystallization enthalpies are given in the inset of Figure 2 and in Table 1. The retarded crystallization might be caused by a lag of mobility of the amorphous phase due to interaction with the nanofiller particles at the interface and in the appearance of a RAF. To validate this hypothesis of lowered mobility at and nearby the interface, StepScan heat capacity measurements in the glass transition region were performed for the differently filled PA6 samples. The result is presented together with the heat capacity of organophilically modified MMT in Figure 3.

Table 1. Measured Quantities during Glass Transition, Melting and Crystallization, for PA6 and Its Nanocomposites Normalized to Polymer Mass and Calculated Values for MAF, CF, and RAF According to Eqs 1−3

	PA6−0.0	PA6−2.2	PA6−4.4	PA6−6.6	PA6−8.8	PA6−19.2	PA6−26.6	PA6−40
$T_g \pm 5$ (°C)	53.5	51.5	51.5	53.5	51.9	53.7	49.2	49.7
$\Delta c_p \pm 0.05$ (J/(g K))	0.15	0.15	0.15	0.15	0.15	0.15	0.15	0.15
$\Delta h_{melt} \pm 5$ (J/g)	68	64	67	66	68	66	51	40
$T_{onset\ cr} \pm 2$ °C	195	195	194	192	190	188	186	177
$\Delta h_{cr} \pm 5$ (J/g)	70	67	69	66	70	68	55	43
MAF ± 0.05	0.33	0.33	0.33	0.33	0.33	0.33	0.33	0.33
CF ± 0.03	0.30	0.29	0.29	0.28	0.29	0.28	0.23	0.18
RAF ± 0.08	0.37	0.38	0.38	0.39	0.38	0.39	0.44	0.49
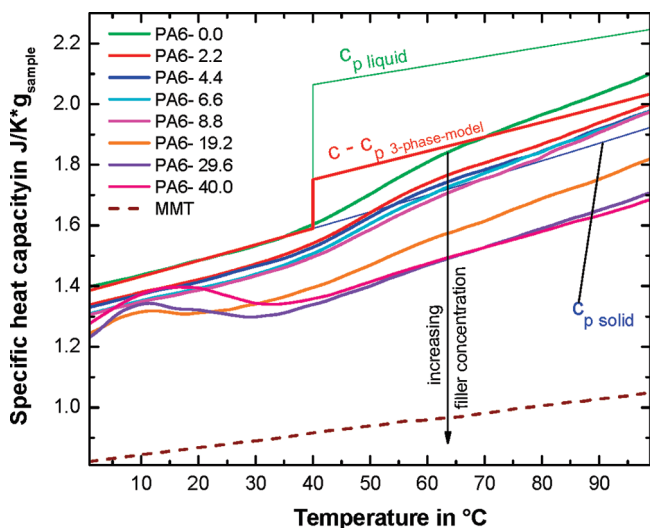
Figure 3. Specific heat capacity per sample mass of PA6, its nanocomposites and organophilically modified MMT in the glass transition region. Specific heat capacity corresponds to normalization by sample mass. Lines for amorphous and solid c_p of PA6 are taken from the ATHAS database.[24]

The relaxation strength at T_g, Δc_p, can be calculated directly from the curves as described for the pure polymer above. Comparison of the Δc_p values for differently filled samples requires normalization to the polymer mass fraction. A direct comparison of the heat capacity curves additionally needs subtraction of the heat capacity contributions of the filler. The heat capacity of the nanocomposite sample (J/K) can be obtained from specific heat capacity (J/(g K)) by multiplying with the sample mass. Multiplying the specific heat capacity (J/(g K)) of the filler (organophilically modified MMT) by the mass of filler in each sample yields the heat capacity contribution of the filler. The difference between the two heat capacities divided by the polymer mass finally results in the specific heat capacity of the polymer fraction in the nanocomposite.

The results of this straightforward procedure are not satisfying because of uncertainties in heat capacity of the nanocomposites and especially the nanofiller. To measure the specific heat capacity of MMT is not an easy task because of the water adsorbed on the large surface, which is evaporating during the measurement even after carefully drying the sample in vacuum. As shown in[33] a simpler correction can be applied. First, the specific heat capacity is recalculated with respect to the polymer fraction by dividing the measured specific heat capacity by (1 − filler content). Next, assuming similar specific heat capacities for the possible RAF originated by the filler, the RAF originated by the crystals and the MAF below the glass transition in the glassy state the curves can be aligned to the specific heat capacity of the PA6 database values below the glass transition by

shifting and rotating. The whole procedure can be applied because of the nearly linear temperature dependence of the specific heat capacity of MMT in the temperature region of interest as shown in Figure 3, dashed line. The results of this correction procedure are presented in Figure 4.

The peak between −20 and +35 °C is due to processes in the nanofiller and occurs only in the samples with the highest filler contents. Because it does not interfere with the glass transition we do not discuss it here in more detail. From the step height at the glass transition, Δc_p, the MAF can be calculated. However, as described above, the tangent method cannot be used due to large contribution of excess heat capacity or changing baseline heat capacity above T_g, e.g., as a result of successive devitrification of RAF. Nevertheless, the individual curves are very similar in the glass transition region. Taking into account the errors in the c_p measurement of about 5% a constant Δc_p can be assumed for the pure PA6 and all nanocomposites. In this case eq 1 yields a constant MAF in all samples.

A proof of this assumption can be provided by annealing experiments at and below T_g. If a fraction of the amorphous polymer in the nanocomposite is immobilized it is expected that the enthalpy relaxation below glass transition is reduced too. Differences in the mobile amorphous fraction which participates in the glass transition at T_g should yield different specific excess heat capacities and excess enthalpies, respectively. Results of the enthalpy relaxation experiments for PA6 and its nanocomposites for annealing at 30 °C for 4 h are presented in Figure 5.

For comparison of the differently filled nanocomposites, the specific excess heat capacities are normalized to the polymer fraction. Finally the area under the excess specific heat capacity is determined by integration from 13 °C, where $c_{p\ excess}$ is nearly zero for all samples, to 120 °C to calculate the specific enthalpy change $\Delta h_{annealing}$ during annealing, see Figure 6.

The line at about 1 J/g suggests a constant value, independent of filler concentration. The large uncertainties of the specific enthalpy change are due to the low amount of polymer in the highly filled samples, which is relaxing during annealing below T_g and causes the endothermic effect. This becomes clear from the following estimation: Samples of about 20 mg were used. For the highest filled sample with 60 wt % filler concentration the remaining polymer mass is about 8 mg. The mobile amorphous fraction of 0.33 corresponds to less than 3 mg of polymeric material, relaxing at T_g. This small amount probed during the annealing results in the large errors.

For calculating CF for each nanocomposite the enthalpy of fusion is needed, which can be derived by integrating heat capacity curves of standard DSC scans in the crystallization or melting region. Enthalpy of fusion for the 100% crystalline sample can be calculated as a function of temperature from ATHAS database values as the difference between the enthalpies for amorphous and crystalline PA6. In the temperature range of interest this difference is nearly constant
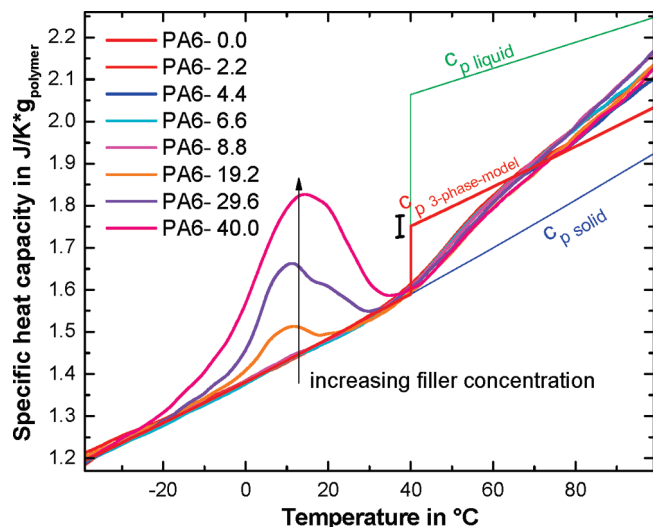
Figure 4. Specific heat capacity per polymer mass of PA6 and its nanocomposites with organophilically modified MMT from StepScan DSC in the glass transition region. Specific heat capacity corresponds to normalization by polymer mass. The lines for amorphous and solid c_p of PA6 are taken from the ATHAS database.[24]
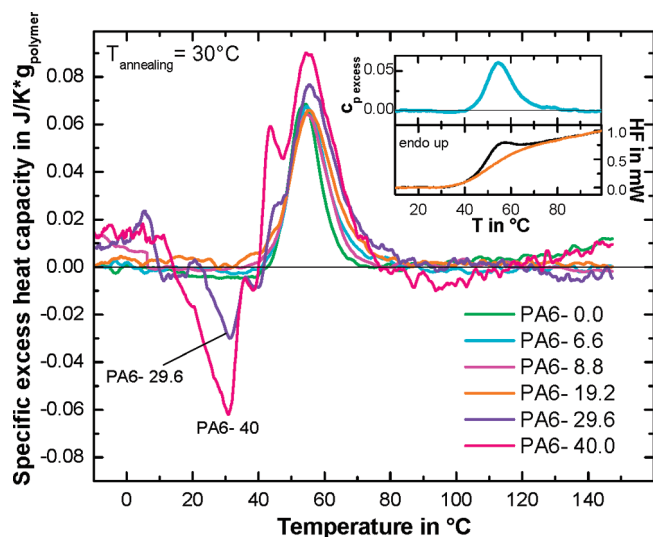

Figure 5. Specific excess heat capacity, $c_{p\ excess}$, per polymer mass in the glass transition region from annealing experiments at 30 °C for 4 h for PA6 and its nanocomposites. The inset shows the measured heat flow rates after annealing and without annealing from DSC scan experiment at 10 K/min (lower part) and the calculated specific excess heat capacity in J/kg$_{polymer}$ for PA6- 6.6 (upper part).

4. Discussion

Comparing the measured curves at T_g, as presented in Figure 4, no significant difference between curves for different
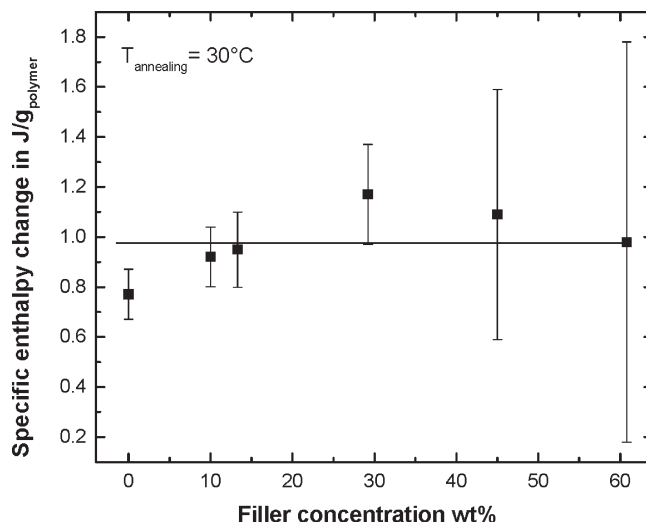

Figure 6. Specific enthalpy change $\Delta h_{annealing}$ in J/g$_{polymer}$ during annealing for 4 h at 30 °C as a function of filler concentration.

filler concentrations can be revealed. The scatter in the curves yields an uncertainty of about 0.05 J/(g K) in c_p, which can be considered as the uncertainty of the measurement. The relaxation strength normalized to the polymer mass is 0.15 J/(g K) and is the same for all nanocomposites and the pure polymer. If for all samples basically the same behavior and same relaxation strength is observed, we obtain at T_g an equal MAF of 0.33 ± 0.1 for all samples. From this finding one can conclude that crystallization in the pure PA6 as well as in the nanocomposites proceeds until mobility in the polymer fraction reaches a certain limit. Independent on the cause of the mobility restriction, RAF due to filler or crystals, crystallization stops if the MAF reaches a value of about 0.33 for all investigated samples.

That the relaxation strength is independent of filler content can be proved by the amount of relaxing polymer below T_g. The specific enthalpy change due to enthalpy relaxation was derived from annealing experiments below T_g. The constant specific enthalpy change (see Figure 6), independent of filler concentration, supports the view of a constant amount of MAF in the pure PA6 and all nanocomposites. Similar results were obtained for isothermally crystallized poly(ethylene therephthalate) (PET).[37]

Considering the values for the crystallization and melting enthalpies in Table 1, it is observed that the values decrease with higher nanofiller concentration. According to eq 2 this observation directly leads to a lower crystalline fraction of the polymer. In Figure 7 CF is presented as points connected by a decreasing line as guide for the eyes.

Assuming a 3-phase-model as described by eq 3 and taking into account the experimentally obtained MAF and CF results in the RAF shown in Figure 7. The constant MAF in combination with the decreasing CF yields an increasing RAF for the higher filled samples. This can be seen from the RAF values, calculated from eq 3 and presented as filled diamonds in Figure 7. The RAF of the polymeric matrix increases from 0.37 to 0.49 for the highest filled sample. Such an increase can only be explained by creation of RAF due to the filler material. Similar to the results obtained with an amorphous polymer matrix,[16] we assume a RAF at the interface between the polymer matrix and the inorganic filler. It is the consequence of lower mobility of the polymer chains at the interface which may have a thickness of a few nanometers as derived in ref 16. The lower mobility is probably caused by chemical interaction between the polymer matrix and the filler at the interface and geometrical constraints like a parallel arrangement of the polymer chains close to the silicate surface.
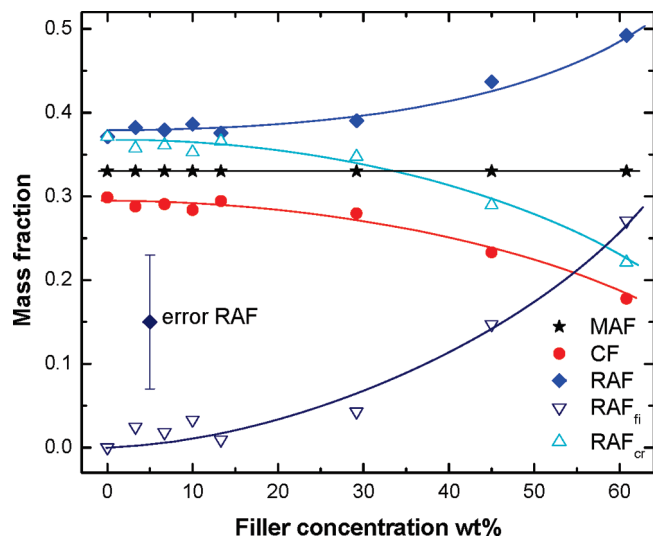
and we calculated crystallinity using the mean value in the temperature interval between 170 and 230 °C $\Delta h_0 = 238$ J/g. We are aware of a small additional uncertainty because we are not applying the exact method given by Mathot, which considers the temperature dependence of the heat of fusion of the infinite crystal.[36] For integration a straight baseline by extrapolating the linear measured heat capacity from the melt was used in accordance to the method proposed by Mathot.[36] From all melting curves the melting enthalpy, Δh, and from eq 2 CF, is available and given in Table 1 beside other parameters.

Figure 7. Mobile amorphous fraction (MAF, ★), crystalline fraction (CF, ●), total rigid amorphous fraction (RAF, ◆), rigid amorphous fraction caused by the crystals (RAF$_{cr}$, △), and rigid amorphous fraction caused by the filler (RAF$_{fi}$, ▽) as a function of MMT concentration. The fractions are given as fraction of the polymer phase in the nanocomposites.

For semicrystalline polymer nanocomposites, one has to assume two different portions of RAF, one originated by the crystals and the second by the filler. According to ref 16, the RAF due to the fillers (RAF$_{fi}$) is stable to high temperatures, up to degradation temperature of PMMA in PMMA/SiO$_2$ nanocomposites. Assuming a similar stability of the RAF$_{fi}$ for the PA6/MMT nanocomposites, it seems to be reasonable to calculate RAF$_{fi}$ in the melt at 250 °C directly from eq 3, taking into account missing CF and considering a superposition of heat capacities of MAF and RAF$_{fi}$ only. Unfortunately, the heat capacities of solid and liquid PA6 at such high temperatures differ only for about 0.12 J/(g K). Considering the minimum uncertainty from exactly done heat capacity measurements of about 2% (0.06 J/(g K)), this method is not reliable because the changes in heat capacity caused by a RAF$_{fi}$ are much too small.

In order to estimate the partition of the RAF between crystals and inorganic filler we assume a constant ratio between RAF$_{cr}$ and the crystalline fraction. As long as the crystalline morphology is the same for the pure PA6 and the nanocomposites this assumption is justified. As shown in Figure 9 lamellar crystals are formed for the nanocomposites too and the assumption is justified. For the pure polyamide the ratio between RAF$_{cr}$ and CF is about 1.2. The rigid amorphous fraction immobilized around the crystals is therefore always larger than the crystalline fraction. Keeping this ratio for the highest filled sample where CF is about 0.18 the RAF$_{cr}$ comes to about 0.22. Taking a constant MAF of 0.33 into account the RAF$_{fi}$ is estimated as 0.27. The analogously calculated values for RAF$_{cr}$ and RAF$_{fi}$ for all nanocomposites are shown in Figure 7 as open triangles up and down, respectively. For the highly filled samples, a remarkable amount of the amorphous material of the polymer phase is immobilized and should change the dynamic behavior of the polymer phase significantly.

A process, which strongly depends on the mobility of the polymer chains, is crystallization. Nucleation, diffusion of crystallizable chain segments, parallel alignment, and attachment to the crystal growth front are only possible, if certain mobility is present. Rigid amorphous parts suppress this mobility and, as shown for pure polycarbonate in,[38] the crystallization process stops due to mobility restrictions of the amorphous material. Similar mobility restrictions can be assumed in the RAF caused
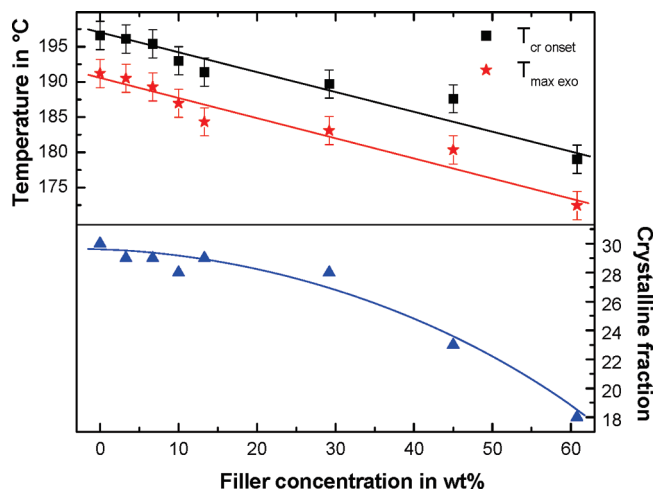

Figure 8. Crystallization onset temperature (T$_{cr\,onset}$ ■), temperature of maximum exothermal effect ($T_{max\,exo}$ ★) and crystallinity of the polymer fraction as a function of nanofiller concentration.

by the nanofiller. For the nanocomposite with the highest filler concentration only 73% of the total polymer is mobile above glass transition where crystallization can appear because of RAF$_{fi}$. It seems reasonable to expect an influence of RAF$_{fi}$ on the crystallization process and finally on crystallinity. The crystallization behavior of PA6 and its nanocomposites on nonisothermal cooling is shown in Figure 2. From the shift of the onset temperature and the maximum temperature of the exothermic peaks toward lower temperatures, presented in Figure 8, a retarded crystallization behavior is observed.

The constant difference between onset temperature ($T_{cr\,onset}$) and temperature of maximum exothermic effect ($T_{max\,exo}$) implies a retarded nucleation followed by a similar crystal growth in all nanocomposites investigated. The constant width of the exothermic effect on cooling supports this view. The retarded onset of crystallization indicates the presence of rigid amorphous material around the filler already in the temperature range of crystallization above 160 °C. This temperature is above any expected glass transition temperature in semicrystalline PA6. According to ref 39, the highest glass transition temperature caused by weak van der Waals interactions of chain segments is the glass transition temperature of the crystals, which is below 150 °C. The origin of the RAF$_{fi}$ must therefore be different. Most probably it is caused by the formation of a much stronger interactions of the polymer with the filler surface. Earlier studies on amorphous polymer/inorganic nanocomposites (PMMA/silica), where RAF can be caused only by the nanofiller, have shown an unexpected high T_g too. The T_g was so high that it was not detected by DSC because of degradation of the polymer before devitrification of the RAF$_{fi}$.[16]

Transmission electron microscope pictures, of which one example is shown in Figure 9, support the existence of a noncrystallizable, rigid amorphous polymer layer around the filler particles. In the micrograph the nanofiller can be seen as black inclusions into the light gray semicrystalline polymer matrix. Crystalline lamellae penetrating the whole polymer matrix can also be observed. Looking in detail to the surrounding of the nanoparticles one recognizes just at the interface between nanofiller and polymer no crystalline lamellae in the polymer matrix, indicated by the white arrow. Lamellae are present only in a distance of about 10 nm from the nanofiller particles. It seems the growing lamellae avoid the space near the nanofiller particle as seen in Figure 9. These observations strongly support the existence of a less mobile region around the nanofillers, where lamellae growth can not proceed.
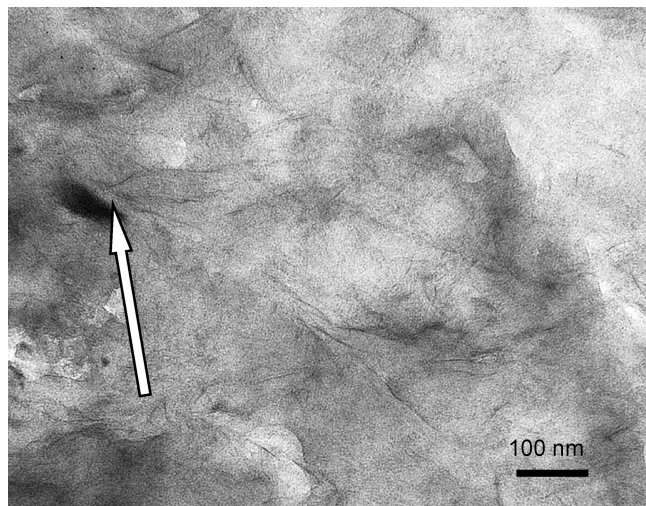
Figure 9. Transmission electron microscopy (TEM) picture of PA6−6.6. Thin sample of about 80 nm thickness was prepared by ultramicrotomy at room temperature using a Leica Ultracut UCT. Micrographs were taken with the 200 keV TEM JEM 2010 (Fa. JEOL).

5. Summary

For polyamide 6/layered silicate nanocomposites a constant remaining mobile amorphous fraction was observed by heat capacity measurements at the glass transition after completed crystallization to a metastable semicrystalline structure. The mobile amorphous fraction was determined by two independent methods:

(i) analyzing the relaxation strength, Δc_p, at T_g;
(ii) enthalpy relaxation from annealing experiments below T_g.

Two different parts of RAF have to be considered by analyzing the heat capacity of semicrystalline nanocomposites, one immobilized at the interface between crystallites and amorphous polymer and the other at the interface between nanoparticles and the polymer.

The RAF caused by the polymer crystals in PA6 is established at or below the crystallization temperature. When RAF_{fi}, caused by the nanofiller, is created is not known yet. It may appear just after melt mixing the nanofiller with the polymer or on cooling from the melt. Properties of RAF_{fi} strongly depend on the temperature of creation.[40] Therefore, an answer to this question is needed but not easy to get. Another open question is related to the organic modifier of the nanofiller. We assume a strong interaction between the polymer and the filler particles, as it was shown for unmodified particles in ref 16, but here it may be the interaction with the organic modifier.

On cooling, crystallization temperature and crystallinity of the polymer phase decreases with increasing filler content. The immobilized layer, RAF_{fi}, around the filler particles and possibly the geometrical constrains caused by the filler particles itself hinder crystallization too. In the studied PA nanocomposites crystallization is retarded and the nanoparticles do not act as nucleating agent. These observations are consistently explained by an immobilized, rigid amorphous fraction around the nanoparticles. Furthermore, crystallization in the pure PA6 as well as in the nanocomposites proceeds as long as certain mobility in the polymer fraction is present. This finding is supported by the constant MAF in the polymer fraction observed for all samples at the end of crystallization.

References and Notes

(1) Alexandre, M.; Dubois, P. *Mater. Sci. Eng. Res.* **2000**, *28*, 1.
(2) Miltner, H. E.; Grossiord, N.; Lu, K.; Loos, J.; Koning, C. E.; Van Mele, B. *Macromolecules* **2008**, *41*, 5753.
(3) Di Maio, E.; Iannace, S.; Sorrentino, L.; Nicolais, L. *Polymer* **2004**, *45*, 8893.
(4) Kim, B.; Lee, S. H.; Lee, D.; Ha, B.; Park, J.; Char, K. *Ind. Eng. Chem. Res.* **2004**, *43*, 6082.
(5) Xu, J. T.; Zhao, Y. Q.; Wang, Q.; Fan, Z. Q. *Polymer* **2005**, *46*, 11978.
(6) Fornes, T. D.; Paul, D. R. *Polymer* **2003**, *44*, 3945.
(7) Homminga, D.; Goderis, B.; Dolbnya, I.; Reynaers, H.; Groeninckx, G. *Polymer* **2005**, *46*, 11359.
(8) Homminga, D.; Goderis, B.; Dolbnya, I.; Groeninckx, G. *Polymer* **2006**, *47*, 1620.
(9) Homminga, D. S.; Goderis, B.; Mathot, V. B. F.; Groeninckx, G. *Polymer* **2006**, *47*, 1630.
(10) Trujillo, M.; Arnal, M. L.; Muller, A. J.; Bredeau, S.; Bonduel, D.; Dubois, P.; Hamley, I. W.; Castelletto, V. *Macromolecules* **2008**, *41*, 2087.
(11) Privalko, V. P.; Dinzhos, R. V.; Privalko, E. G. *Thermochim. Acta* **2005**, *432*, 76.
(12) Privalko, V. P.; Lipatov, Y. S.; Kercha, Y. Y. *Polym. Sci. U.S.S.R.* **1970**, *12*, 1520.
(13) Lipatov, Y. S.; Privalko, V. P. *Polym. Sci. U.S.S.R.* **1972**, *14*, 1843.
(14) Fragiadakis, D.; Pissis, P. *J. Non-Cryst. Solids* **2007**, *353*, 4344.
(15) Logakis, E.; Pandis, C.; Peoglos, V.; Pissis, P.; Stergiou, C.; Pionteck, J.; Pötschke, P.; Miccaronuscaroník, M.; Omastová, M. *J. Polym. Sci., Part B: Polym. Phys.* **2009**, *47*, 764.
(16) Sargsyan, A.; Tonoyan, A.; Davtyan, S.; Schick, C. *Eur. Polym. J.* **2007**, *43*, 3113.
(17) Suzuki, H.; Grebowicz, J.; Wunderlich, B. *Br. Polym. J.* **1985**, *17*, 1.
(18) Wunderlich, B. *Prog. Polym. Sci.* **2003**, *28*, 383.
(19) Koh, Y. P.; McKenna, G. B.; Simon, S. L. *J. Polym. Sci., B: Polym. Phys.* **2006**, *44*, 3518.
(20) Sarge, S. M.; Hemminger, W.; Gmelin, E.; Hohne, G. W. H.; Cammenga, H. K.; Eysel, W. *J. Therm. Anal.* **1997**, *49*, 1125.
(21) Petrie, S. E. B. In *Physical structure of the amorphous state*,; Allen, G., Petrie, S. E. B., Eds.; Marcel Dekker: New York, 1975.
(22) Wunderlich, B. *J. Appl. Polym. Sci.* **2007**, *105*, 49.
(23) Wunderlich, B. *Thermal Analysis of Polymeric Materials*; Springer: Berlin, 2005.
(24) Wunderlich, B. *Pure Appl. Chem.* **1995**, *67*, 1019.
(25) Schick, C. *Temperature modulated differential scanning calorimetry (TMDSC)*—*Basics and applications to polymers*; In *Handbook of thermal analysis and calorimetry*; Brown, M. E., Gallagher, P. K., Eds.; Elsevier, Amsterdam, 2002; Vol. *3*, pp 713−810.
(26) Grebowicz, J.; Suzuki, H.; Wunderlich, B. *Polymer* **1985**, *26*, 561.
(27) Wurm, A.; Merzlyakov, M.; Schick, C. *J. Therm. Anal. Calorim.* **2000**, *60*, 807.
(28) Schick, C.; Wurm, A.; Mohammed, A. *Thermochim. Acta* **2002**, *392−393*, 303.
(29) Schick, C.; Wurm, A.; Mohammed, A., *Vitrication and Devitrication of the Rigid Amorphous Fraction in Semicrystalline Polymers Revealed from Frequency Dependent Heat Capacity*; Springer: Berlin, 2003; Lecture Notes in Physics, Vol. *606*, p 252−275.
(30) Androsch, R.; Wunderlich, B.; Radusch, H. J. *J. Therm. Anal. Calorim.* **2005**, *79*, 615.
(31) Androsch, R.; Wunderlich, B. *Macromolecules* **2001**, *34*, 5950.
(32) Donth, E., *Glasübergang*; Akademieverlag: Berlin, 1981.
(33) Sargsyan, A. Quantification of the Immobilized Fraction in Polymer Inorganic Nanocomposites. Ph.D. Thesis, Universität Rostock: Rostock, Germany, **2007**.
(34) Hodge, I. M. *J. Non-Cryst. Solids* **1994**, *169*, 211.
(35) Adamovsky, S.; Schick, C. *Thermochim. Acta* **2004**, *415*, 1.
(36) Mathot, V. B. F., *Calorimetry and Thermal Analysis of Polymers*; Hanser Publishers: München, Germany, 1994.
(37) Schick, C.; Donth, E. *Phys. Scr.* **1991**, *43*, 423.
(38) Schick, C.; Wurm, A.; Mohammed, A. *Colloid Polym. Sci.* **2001**, *279*, 800.
(39) Wunderlich, B. *J. Therm. Anal. Calorim.* **2008**, *93*, 7.
(40) Schick, C.; Dobbertin, J.; Potter, M.; Dehne, H.; Hensel, A.; Wurm, A.; Ghoneim, A. M.; Weyer, S. *J. Therm. Anal.* **1997**, *49*, 499.